Bull Earthquake Eng (2011) 9:717–739
DOI 10.1007/s10518-011-9248-4

ORIGINAL RESEARCH PAPER

Separation of source and site effects by generalized inversion technique using the aftershock recordings of the 2009 L'Aquila earthquake

G. Ameri · A. Oth · M. Pilz · D. Bindi · S. Parolai · L. Luzi · M. Mucciarelli · G. Cultrera

Received: 28 October 2010 / Accepted: 4 February 2011 / Published online: 23 March 2011

Abstract We exploit S-wave spectral amplitudes from 112 aftershocks ($3.0 \leq M_L \leq 5.3$) of the L'Aquila 2009 seismic sequence recorded at 23 temporary stations in the epicentral area to estimate the source parameters of these events, the seismic attenuation characteristics and the site amplification effects at the recording sites. The spectral attenuation curves exhibit a very fast decay in the first few kilometers that could be attributed to the large attenuation of waves traveling trough the highly heterogeneous and fractured crust in the fault zone of the L'Aquila mainshock. The S-waves total attenuation in the first 30 km can be parameterized by a quality factor $Q_S(f) = 23 f^{0.58}$ obtained by fixing the geometrical spreading to 1/R. The source spectra can be satisfactorily modeled using the omega-square model that provides stress drops between 0.3 and 60 MPa with a mean value of 3.3 ± 2.8 MPa. The site responses show a large variability over the study area and significant amplification peaks are visible in the frequency range from 1 to more than 10 Hz. Finally, the vertical component of the motion is amplified at a number of sites where, as a consequence, the horizontal-to-vertical spectral

G. Ameri (✉) · L. Luzi
Istituto Nazionale di Geofisica e Vulcanologia, via Bassini 15, 20133 Milano, Italy
e-mail: ameri@mi.ingv.it

A. Oth
European Center for Geodynamics and Seismology, rue Josy Welter 19, 7256 Walferdange, Luxembourg

M. Pilz · S. Parolai
Section 2.1, Telegrafenberg, Deutsches GeoForschungsZentrum GFZ, Helmholtzstraße 7, 14467 Potsdam, Germany

D. Bindi
Centre for Disaster Management and Risk Reduction Technology (CEDIM), Deutsches GeoForschungsZentrum GFZ, Helmholtzstraße 7, 14467 Potsdam, Germany

M. Mucciarelli
Università della Basilicata, via dell'Ateneo Lucano 10, 85100 Potenza, Italy

G. Cultrera
Istituto Nazionale di Geofisica e Vulcanologia, via di Vigna Murata 605, 00143 Roma, Italy

ratios (HVSR) method fails in detecting the amplitude levels and in few cases the resonance frequencies.

Keywords L'Aquila Sequence · Generalized inversion technique · Site effects · Source parameters · Seismic attenuation

1 Introduction

In the first days after the 6 April 2009 L'Aquila earthquake ($M_w = 6.3$), a number of temporary stations, operated by different institutions, were deployed in the epicentral area (Cultrera et al. 2009; Bergamaschi et al. this issue). Most of them were concentrated in the middle Aterno valley (i.e., southeast to L'Aquila) mainly because it is there where the most severely damaged villages were located and the geologic and geomorphologic characteristics made the valley prone to possible ground-motion amplifications. The temporary network recorded a considerable number of aftershocks and therefore, allows for the estimation of local amplification phenomena through empirical techniques and the comparison of the results obtained with different approaches. Preliminary results on empirically-based site responses for the middle Aterno valley were presented by Cultrera et al. (2009) in terms of horizontal-to-vertical spectral ratios from earthquake recordings (HVSR; Lermo and Chávez-García 1993). The authors report a very large variability of the seismic response of the examined sites, with amplifications mainly in frequency band 1–5 Hz.

Studies dedicated to the comparison of different site response estimation techniques (e.g., Field and Jacob 1995; Bonilla et al. 1997; Parolai et al. 2004) generally indicate that the HVSR and reference site methods (e.g., Standard Spectra Ratios, SSR, Tucker and King 1984) are capable to consistently estimate the fundamental resonance frequency of a site, but the HVSR estimates generally provide different levels of amplification. Moreover, if both the vertical and horizontal components are amplified at the same resonance frequencies, the HVSR method fails.

Bergamaschi et al. (this issue) used data from 18 earthquakes recorded at 14 of the deployed temporary stations to evaluate the HVSR for each site and the SSR between each site and a reference station. The SSR method is based on the condition that, for an event, a record from the reference site (a station installed on outcropping rock, assumed to be amplification-free) contains the same source and propagation effects as records from the other sites. It is implied that differences in the observed ground motion at the sites is solely due to the different near-surface amplification. However, this assumption is reasonable only when data from dense, local arrays are used, that is, when the source-to-site paths are similar.

An alternative reference site method that extends the SSR approach to large networks and thus overcomes some of its limitations is the generalized inversion technique (GIT, Andrews 1986; Castro et al. 1990; Parolai et al. 2000). In this method, the Fourier amplitude spectra (FAS) from earthquake records are jointly inverted in order to separate their source, path and site contributions.

Bindi et al. (2009) applied the GIT scheme to the L'Aquila earthquake data considering strong-motion records from 13 events with $M_w \geq 4$. This study is an extension of Bindi et al. (2009) and presents several differences with respect to their paper: (i) we consider a substantially larger number of events; (ii) we use temporary accelerometric and velocimetric stations, whereas they only used permanent stations from the Italian Strong Motion Network (RAN); iii) the magnitude-distance distribution of the two datasets is different, since our dataset samples also smaller magnitudes ($M_w < 4$) and shorter hypocentral distances.

In this article we describe the results obtained applying the GIT to the data recorded during the first 40 days after the L'Aquila mainshock by the temporary network deployed in the Aterno valley. We first present the dataset and discuss the processing of the records, then we discuss the inversion results in terms of attenuation functions, source spectra and site responses. The S-waves total attenuation of ground motion as a function of distance and frequency is parameterized in terms of geometrical spreading and quality factor $Q_S(f)$. The obtained nonparametric source spectra are interpreted using the omega-square model (Brune 1970) and the retrieved seismic moments and stress drops are discussed and compared with other studies. Finally, we derive the site response functions from both horizontal and vertical components of FAS and compare them with HVSR.

The considered source-to-station distances (mostly within 35 km) are on average shorter than the usual range of GIT applications (e.g., Parolai et al. 2004; Castro et al. 2008; Bindi et al. 2009), and the inter-station distance is, in some cases, smaller than 1 km. Under such condition of short and similar ray paths, the method could fail in separating simultaneously the effect of site, source, and attenuation. Thus, one of the aims of this paper is to also test the reliability of GIT results in such setting.

2 Dataset

After the 6 April L'Aquila mainshock (Chiarabba et al. 2009), 33 seismic stations (both accelerometers and velocimeters) were deployed in the Aterno river Valley in order to record the aftershocks and to characterize the seismic response of the area (see Cultrera et al. 2009 and Bergamaschi et al. this issue, for a detailed description of the experiment). The collected dataset includes the recordings from more than 100 earthquakes with magnitudes larger than 3 that occurred from April 7th to May 15th 2009 and were located within 30 km from the L'Aquila mainshock epicenter. For the purpose of this study, we reduced the collected dataset excluding saturated velocimetric signals, stations affected by technical problems (i.e., GFZ02, GFZ03, GFZ06) and stations that are installed inside buildings. After this selection, about 1,200 three-component records were available from 23 temporary stations belonging to the different institutions that participated in the survey (Fig. 1; Table 1). The velocimetric stations were equipped with either Lennartz LE-3D/5s or LE-3D/1s sensors (INGV stations) and with Mark-L4C-3D sensors (GFZ stations). The accelerometric stations were equipped with EpiSensor. Figure 2 (upper panel) shows the distribution of records considered in this study as a function of event and station identification (ID) numbers (black and gray symbols represent velocimetric and accelerometric stations, respectively). Note that the distribution of records with time is quite heterogeneous as some stations operated for the entire time period considered while others were deployed only for some days. The local magnitudes (M_L) range from 3.0 to 5.3 and the hypocentral distances from 8 to 50 km. Most of the records are related to $M_L \leq 4$ events and hypocentral distance between 10 and 30–35 km (Fig. 2, lower plots). The M_L values and seismic events localizations are obtained from the INGV-CNT Bulletin (http://cnt.rm.ingv.it).

The velocity records were first corrected for the instrumental response, the mean from the whole signal removed and differentiated to acceleration. Then, time windows starting 0.5 s before the S-wave onset and ending when 90 percent of the total energy after the S-wave onset has been released, with a minimum and maximum allowed duration of 5 and 15 s, respectively, have been extracted and tapered with a 5% Hanning window. For the selected windows, the acceleration FAS have been calculated and smoothed using the Konno and Ohmachi (1998) algorithm, fixing the smoothing parameter b to 40. The spectral ampli-

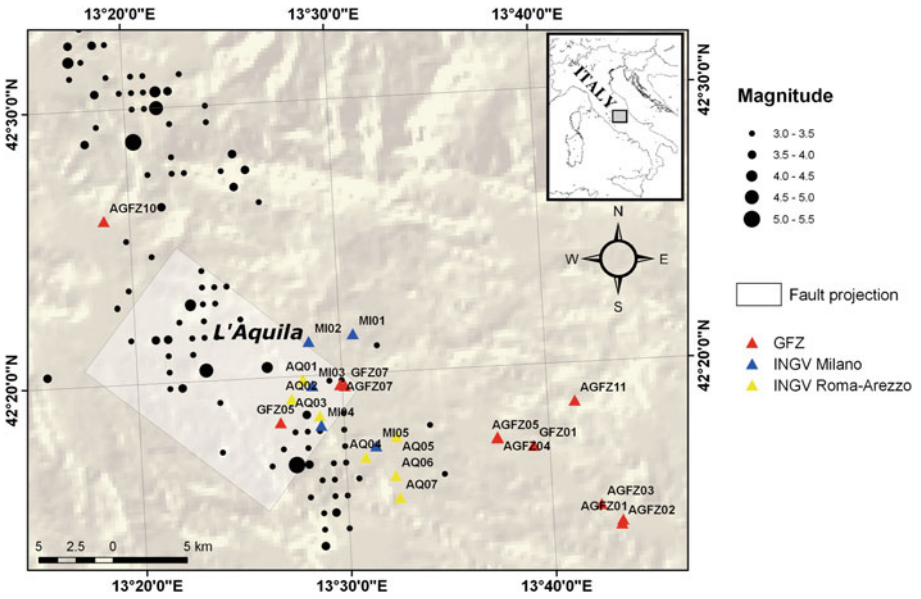

Fig. 1 Map of the study area. The temporary seismic network installed in the Aterno valley is shown by *triangles*. *Circles* are the earthquakes used in this study. The *gray-shaded rectangle* shows the surface projection of the L'Aquila mainshock fault

tudes are analyzed at 36 frequencies, equally spaced on a logarithmic scale over the range 0.5–30 Hz. Pre-event noise windows of equal length as the signal windows were used to compute the signal-to-noise ratios (SNR), and, at each frequency point, only records with a SNR larger than 3 were retained. Figure 3 shows examples of SNR calculated for three stations located in different positions over the study area and equipped with different instrumentation systems. AQ06 and GFZ05 are velocimetric stations whereas MI01 is accelerometric. Moreover MI01 and GFZ05 are installed on outcropping rock while AQ06 is located on the alluvial deposits of the Aterno river (see Fig. 1 and Bergamaschi et al. this issue). The SNR are high with median values between 10 and 1,000 and only few frequency points with a ratio smaller than 3. For the whole data set, the number of selected spectral amplitudes, based on SNR > 3, spans from 1,124 at 0.5 Hz to 1,161 at 10 Hz.

3 Methods

We apply a nonparametric generalized spectral inversion scheme originally introduced by Castro et al. (1990) in order to separate the FAS into their source, path and site contributions. Since the technique is well known and has been applied in a large number of studies throughout the past years, we only briefly summarize it here and refer the reader to the literature for a more detailed discussion and description of the matrix system (e.g. Castro et al. 1990; Parolai et al. 2000, 2004; Oth et al. 2008, 2009, 2010).

The Fourier amplitude spectra of ground motion can be expressed as:

$$U_{ij}(f, R_{ij}) = S_i(f) \cdot A(f, R_{ij}) \cdot G_j(f), \tag{1}$$

Table 1 List of stations used in this study

Station	Locality	Lat (°)	Lon (°)	# Records
AQ01	Bazzano-Onna	42.331500	13.468000	88
AQ02	Monticchio	42.320100	13.458333	59
AQ03	Fossa	42.308883	13.480433	20
AQ04	Casentino	42.282533	13.516267	70
AQ05	S. Demetro nei Vestini	42.293900	13.542383	36
AQ06	Villa Sant'Agelo	42.270250	13.539950	88
AQ07	Stiffe (cavern)	42.256950	13.542633	20
MI01	Pescomaggiore	42.358035	13.50977	97
MI02	Paganica	42.354487	13.47428	97
MI03	Onna	42.327415	13.47569	54
MI04	Fossa	42.303127	13.48139	84
MI05	S Eusanio Forconese	42.289473	13.52526	92
AGFZ01	Navelli Piccioli square	42.236576	13.726637	50
AGFZ02	Navelli Town Hall	42.238426	13.727509	67
AGFZ03	Civita Retenga	42.246550	13.706133	14
AGFZ04	Castelnuovo castle	42.294799	13.629832	16
AGFZ05	Castelnuovo road	42.294333	13.628965	16
AGFZ07	San Gregorio	42.327133	13.498450	28
AGFZ10	Pizzoli school	42.43296	13.31227	10
AGFZ11	Castelvecchio Calvisio	42.31012	13.68884	18
GFZ01	S. Pio	42.284133	13.653317	34
GFZ05	Civita di Bagno	42.306000	13.448250	55
GFZ07	S. Gregorio Agriturismo	42.326383	13.502183	62

The number of records considered in the inversion for a frequency of 5.63 Hz is reported

where $U_{ij}(f, R_{ij})$ stands for the spectral amplitude observed at the jth station and caused by the ith earthquake, R_{ij} is the hypocentral distance, $S_i(f)$ stands for the source spectrum of the ith earthquake, $A(f, R_{ij})$ is a non-parametric function of distance and frequency accounting for the path effects, and $G_j(f)$ is the site response function of the jth station. Equation (1) can be turned into a linear problem by simply taking the logarithm:

$$\log_{10} U_{ij}(f, R_{ij}) = \log_{10} S_i(f) + \log_{10} A(f, R_{ij}) + \log_{10} G_j(f). \tag{2}$$

Equation (2) represents a linear system of equations $\mathbf{Ax} = \mathbf{b}$, where $\mathbf{b}$ is the data vector consisting of the logarithmic spectral amplitudes, $\mathbf{x}$ is the vector containing the model parameters and $\mathbf{A}$ is the system matrix relating them. We solve this linear system using singular value decomposition (Menke 1989).

Some constraints always need to be applied in order to be able to solve the system. The attenuation operator is expressed as a nonparametric function of (binned) distance. The attenuation is set at a given reference distance R_0 (in our case 8 km, which is the smallest hypocentral distance present in our dataset) to be equal to unity, i.e., $A(f, R_0) = 1$. Furthermore, we constrain the attenuation operator to be a smooth function of distance (i.e., small second derivative, Castro et al. 1990).

As Andrews (1986) pointed out, one further constraint is required in order to remove an unconstrained degree of freedom between source spectra and site response functions. This constraint may either be imposed on one (or several) source spectra or/and site response functions. In our case, we decided to constrain the site response at one specific rock site to be equal to unity. Based on field evidences (i.e., the station is installed on outcropping rock) and on results from horizontal-to-vertical spectral ratios (HVSR), presented in the Results section, we selected GFZ05 as reference station for rock site conditions.

We solve Eq. (2) in one step as described by Oth et al. (2010), who showed that with this scheme, stable attenuation functions can be retrieved whatever reference condition is used for the source/site part. In order to assess the stability of the inversion results, we perform 100 bootstrap inversions at each frequency point following the procedure detailed in Parolai et al. (2000, 2004) and Oth et al. (2008, 2009), and calculate mean as well as standard errors for the model parameters.

Besides the nonparametric approach for generalized spectral inversion used in this article, there are also parametric variants followed by other authors in the literature, the latter involving a priori parametric descriptions of the attenuation operator (e.g. Castro et al. 1990; Salazar et al. 2007) and sometimes also of source spectral shape (e.g. Drouet et al. 2008). However, we prefer to follow the nonparametric approach since, if the functional forms of attenuation operator (and source spectra) are constrained a priori, strong model assumptions are imposed on the dataset. Consequently, deviations from these assumptions will simply be shifted into the residuals (respectively the site amplification functions) and may therefore, bias the obtained results. In contrast, such assumptions are not imposed in the nonparametric scheme, and the fit between the nonparametric inversion results and a given functional model can be assessed a posteriori.

Finally, we compare our results from the spectral inversion with the standard site response estimators used throughout the literature, i.e., HVSR from ambient noise (only in the case of velocimetric sensors) and from the same earthquake data as used for the inversion. The HVSR site response estimator simply consists in the ratio between the horizontal and vertical component FAS of the S-wave windows. The HVSR method was made popular by Nakamura (1989) for use with ambient noise recordings and was first applied to earthquake records by Lermo and Chávez-García (1993). In this study, for the horizontal spectral amplitude the vector sum of the north-south and east-west components is used $\left(\text{i.e. } \sqrt{NS^2 + EW^2}\right)$ in the calculations.

4 Results

4.1 Spectral attenuation with distance

In order to describe the spectral attenuation as a nonparametric function of distance, we need to discretize the distance range considered in this study (i.e., 8–50 km) into a number of bins, where it is desirable to have a comparable number of data points in each bin. We noticed in several test runs that attenuation is very pronounced at short distances (in the range 8–14 km) and that, if the bins in this distance range are chosen too large, the smoothing constraint suppresses the quite large variations over this comparatively short distances and leads to inappropriate attenuation functions over that range. Since we have a large number of data points at short distances (Fig. 2), we used small bins of 0.5 km width in the distance range 8–14 km, whereas we increased the bin size to 2 km in the range 14–40 and to 5 km in the

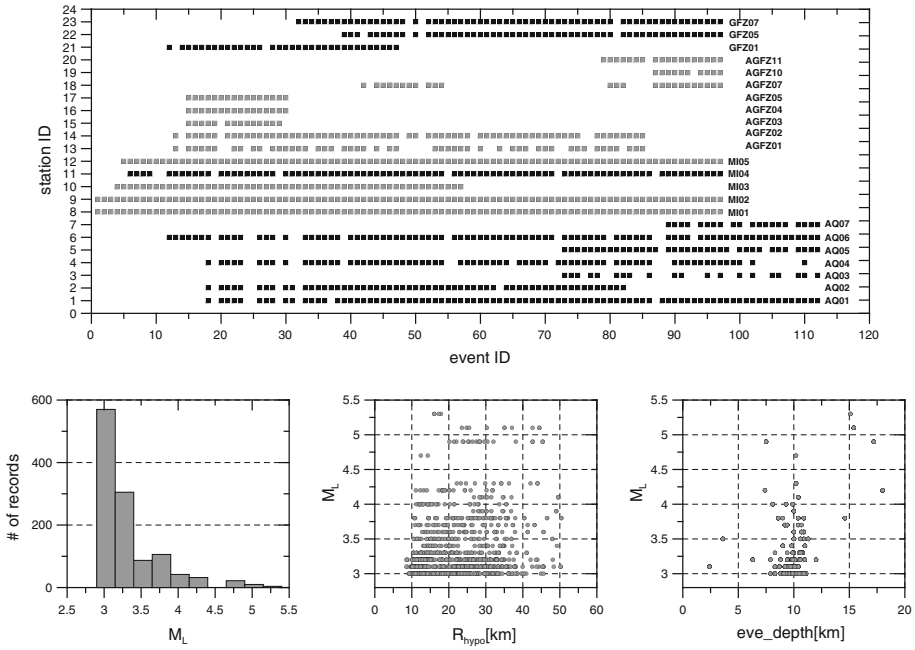

Fig. 2 Dataset used in this study. *Top*: distribution of records divided for the different temporary stations deployed in the area (*black*: velocimetric stations, *gray*: accelerometric stations). *Bottom*: magnitude/distance/depth distribution of records (from left to right). Local magnitudes (M_L) are obtained from the INGV-CNT Bulletin (http://cnt.rm.ingv.it)

range 40–50 km (where the number of data points begins to become rather sparse). This way, we are also able to reproduce quite steep decays of spectral amplitudes at short distances with the inverted attenuation functions.

Figure 4 shows the nonparametric attenuation functions at three sample frequencies together with the residual spectral amplitudes after removing source and site effects as obtained from the inversion (see next sections). The attenuation functions show a very steep decay in the first few kilometers (i.e. $R < 13$ km), observed at all the examined frequencies. At larger distances the attenuation rate changes and for $R > 30$–35 km the curves start to flatten (or even to slope upward) depending on the considered frequency. This latter feature is generally explainable, in certain distance ranges, due to critically reflected arrivals from the Moho. Although the Moho depth is quite variable and recent studies from teleseismic receiver functions (Piana Agostinetti and Amato 2009) report relatively shallow Moho depth (about 30–35 km) for the central Apennines, such arrivals are generally observed at larger distances of about 50–70 km (Ponziani et al. 1995; Bindi et al. 2004, 2009). The behavior of the nonparametric curves, for the 36 frequencies considered in this study (Fig. 5a), suggests that the reflections and refractions from crustal interfaces, possibly shallower than the Moho, are significant in the investigated area already for distances between 30 and 50 km.

In Fig. 5a the attenuation curves are also compared with R^{-1} and R^{-3} decays representing the body waves geometrical attenuation for far-field and near-field terms, respectively (Aki and Richards 1980). For distances smaller than about 13 km the data seem to attenuate as R^{-3} whereas at larger distances the R^{-1} decay is preferred. The near-field terms are usually dominant in the ground motion at distances of the order of few source dimensions and at low

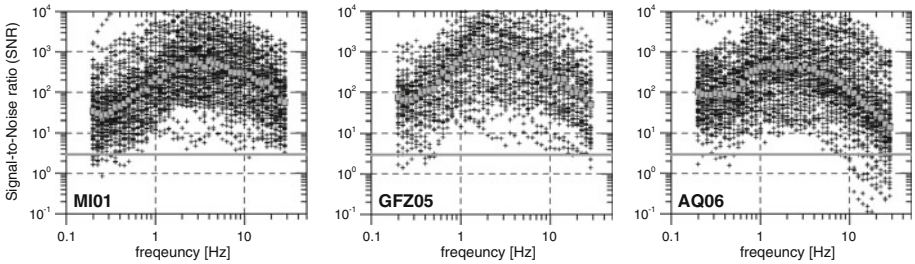

Fig. 3 Signal-to-noise ratios (*SNR, black crosses*) versus frequency for three of the considered stations. The median SNR value at each frequency is shown by *gray dots*

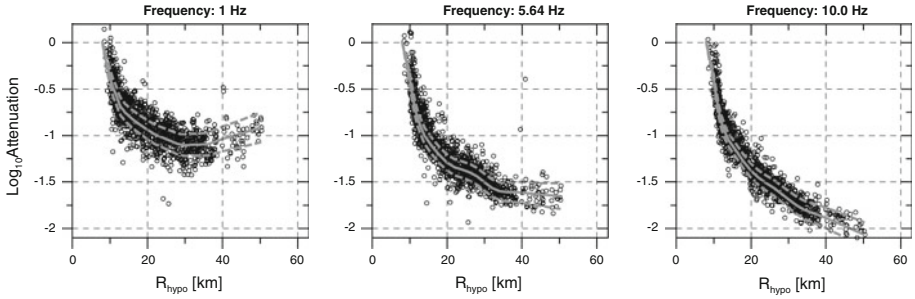

Fig. 4 Nonparametric attenuation functions derived for three different frequencies (mean ±1 standard deviation). Black *circles* are residuals calculated after removing source and site contributions to the spectral amplitudes

frequencies (roughly below 1 Hz). However, in this case, due to the magnitudes (and consequent source size) of the events related to the shortest distances in the dataset (8–13 km), far-field terms are expected to be dominant in the ground motion. Alternatively, the strong attenuation could be caused by attenuation properties of the shallow crust. Indeed, the ray paths from earthquakes with source-to-site distance smaller than 13 km are mostly travelling through the fault zone of the L'Aquila mainshock directly upward to the middle Aterno valley stations. As a consequence, the fractured crust around the hypocentral area of the mainshock can cause the observed large attenuation of S-waves.

The nonparametric attenuation curves for $R \leq 30$ km, where monotonic attenuation with distance occurs, are described in terms of geometrical spreading and anelastic attenuation, considering the following model:

$$A(f,r) = \left(\frac{R_0}{R}\right)^n \exp\left[\frac{-\pi f (R - R_0)}{\beta Q_S}\right], \tag{3}$$

where n is the geometrical spreading coefficient, $\beta = 3.2$ km/s is the assumed mean shear-wave velocity (e.g. Rovelli et al. 1988), and Q_S is the frequency-dependent quality factor. Since a strong trade-off usually exists between n and $Q_S(f)$ in solving Eq. (3), we only invert for $Q_S(f)$ by constraining n to a fixed value. Because of the previous discussion, recognizing that the usual $n = 1$ might not be appropriate to describe the geometrical attenuation in the short distance range (Fig. 5a), we considered two alternative models of the geometrical spreading: (1) a single decay rate with $n = 1$ and (2) two decay rates with $n = 3$ up to 13 km and $n = 1$ beyond that distance.

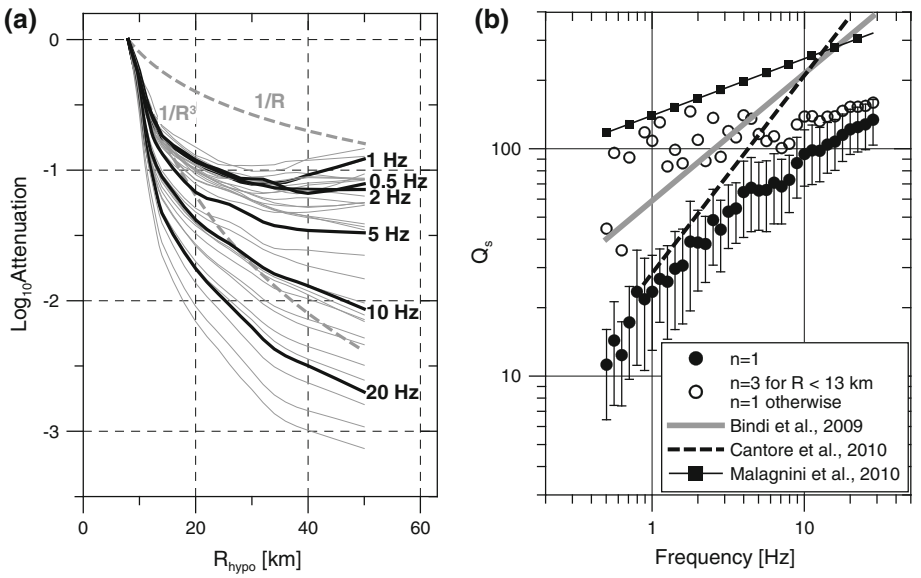

Fig. 5 **a** Nonparametric spectral attenuation versus distance at each frequency (*gray curves*). Six representative frequencies are shown with *black lines*. R^{-1} and R^{-3} decays are shown by the *dashed gray lines*. **b** Frequency dependence of Q_S for distances between 8 and 30 km. *Black dots* and *error bars* indicate the Q_S estimates at each individual frequency considering a single geometrical spreading decay with $n = 1$. *White dots* are Q_S estimates at each individual frequency considering a distance-dependant geometrical spreading. The $Q_S(f)$ values obtained by Bindi et al. (2009), Cantore et al. (2011) and Malagnini et al. (2010) are also reported

After correcting the nonparametric attenuation function for each of the two geometrical spreading decays, we estimated two $Q_S(f)$ models shown in Fig. 5b. When $n = 1$ is used, by fitting a power function to $Q_S(f)$, the best least-squares solution is given by $Q_S(f) = 23.28(\pm 1.61)\, f^{0.58(\pm 0.04)}$. On the other hand, if the distance-dependant geometrical spreading is used, the $Q_S(f)$ values are more scattered assuming larger values roughly between 100 and 200 and showing a weak dependence on frequency (at least for frequency > 1 Hz). Figure 5b also reports the $Q_S(f)$ values by Bindi et al. (2009) for R < 50 km, in the same area (i.e. $Q_S(f) = 59 f^{0.56}$ for $n = 1$). Although their estimates are somehow shifted towards larger Q_S values, thus prescribing smaller attenuations, it has to be taken into account that their dataset is substantially different from the one we used in this study. In particular, they considered 13 events with magnitude larger than 4 with the bulk of records at distances larger than 20 km. In contrast, we considered also smaller magnitudes and a large number of data in the distance range 10–30 km. Regarding the frequency dependence of Q_S, almost the same exponent value is found in both studies, when $n = 1$ is considered. Figure 5b also reports the Q_S models obtained by Cantore et al. (2011) and by Malagnini et al. (2010). The former has been derived applying the GIT method to a local dataset collected in the epicentral region of the 1980 Irpinia earthquake (Southern Italy) and characterized by similar magnitude-distance distribution to the one considered in this study (although we used a larger number of data). Interestingly the Q_S values are similar to our model up to 3 Hz, thus providing quite large attenuation, while at higher frequencies the Cantore et al. (2011) model suggest larger values (i.e., smaller attenuation). Malagnini et al. (2010) studied the attenuation in the Central Apennines using a dataset of 170 foreshocks and aftershocks

of the L'Aquila earthquake ($2.8 \leq M_w \leq 6.15$) recorded by the National Digital Seismic Network (http://cnt.rm.ingv.it/) at distances up to 200 km. The authors derived a $Q_S(f)$ model adopting a distance-dependent geometrical spreading with $n = 1.1$ below 10 km, $n = 1.0$ between 10 and 30 km and $n = 0.7$ beyond 30 km. Although their model prescribe smaller attenuation, the frequency dependence and the Q_S values are similar to the one we obtain adopting the distance-dependent geometrical spreading (white dots in Fig. 5b). Considering the different crustal volumes and frequency bands investigated by the different authors, the comparison presented in Fig. 5b makes us confident about the $Q_S(f)$ model estimated in this study.

4.2 Source spectra

Having discussed the most important features of the nonparametric attenuation functions, we now turn our attention to the source spectra obtained from the GIT inversion. In order to derive the source parameters (i.e. seismic moments and corner frequencies) of the 112 earthquakes in our dataset (see Appendix Table 2), we fitted the omega-square model (Brune 1970) to the inverted nonparametric acceleration source spectra using non-linear least squares (Seber and Wild 2003):

$$S(f) = C M_0 (2\pi f)^2 \frac{1}{1 + \left(\frac{f}{f_C}\right)^2}, \tag{4}$$

with the constant C being

$$C = \frac{\Re_{\theta\varphi} F V}{4\pi\rho\beta^3 R_0}, \tag{5}$$

where $\Re_{\theta\varphi}$ is the average radiation pattern for S-waves set to 0.55, $V = \sqrt{2}$ accounts for the partition of S-wave energy onto two horizontal components, $F = 2$ is the free-surface amplification and $\rho = 2.8$ g/cm^3 is the density. $R_0 = 8$ km represents the reference distance, M_0 denotes the seismic moment and f_C is the corner frequency.

The nonparametric source functions obtained in the inversion are presented in Fig. 6 for six events approximately spanning the range of considered magnitudes and the entire time period. Each spectrum is compared with the fitted omega-square model, showing that the nonparametric spectra can satisfactorily be explained using this source model. For each plot, the moment magnitude (M_w, derived from seismic moment using Hanks and Kanamori 1979) and the f_c estimated in the least-square regression are reported.

Figure 7 shows the seismic moments (estimated in the inversion) versus local magnitudes (M_L) from the INGV-CNT seismic bulletin for all events in the dataset. Note that, in order to avoid biases in the estimation of the source parameters for three events (indicated by stars in Fig. 7) having $M_L > 4$ but only few records (less than 5), we constrained their seismic moments to the values provided by Regional Centroid Moment Tensor, RCMT (http://www.bo.ingv.it/RCMT/). The best least-squares fit is reported in Fig. 7 and it is compared with the relation obtained by Castello et al. (2007) considering data from the INGV-CNT bulletin and seismic moments from RCMT between 1997 and 2002. The two relations are in good agreement in their range of validity; they start to diverge toward smaller M_L where the GIT results provide slightly larger seismic moments. Some of the estimated M_0 for M_L between 3 and 4 present, however, remarkable uncertainties due to the small number of records available

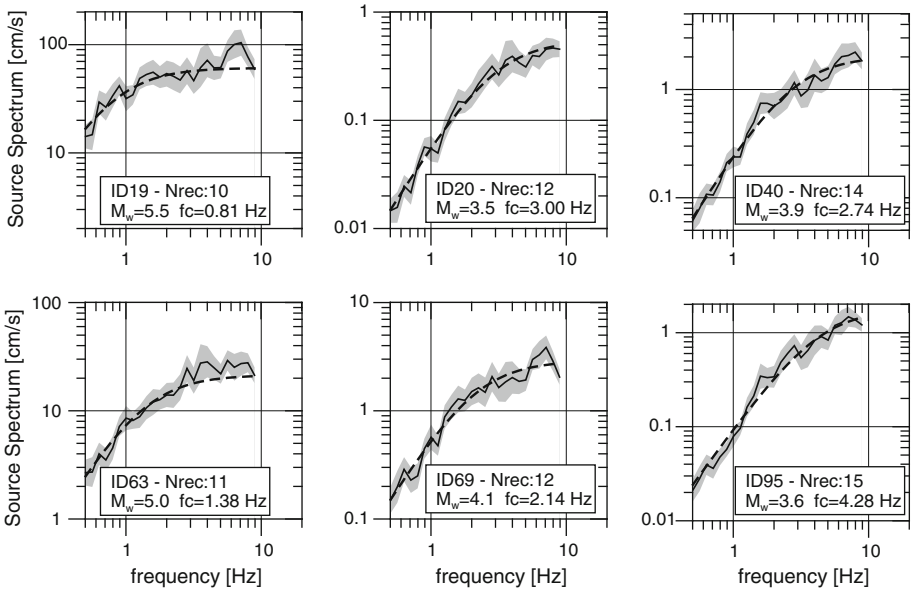

Fig. 6 Examples of fit between the inverted source spectra (*continuous lines*) with relative standard deviation (*shaded area*) and omega-square models (*dashed lines*). For each event the number of records used in the inversion (Nrec), the moment magnitude (M_W) and the corner frequency (*fc*) estimated from the fitted omega-square spectra are reported

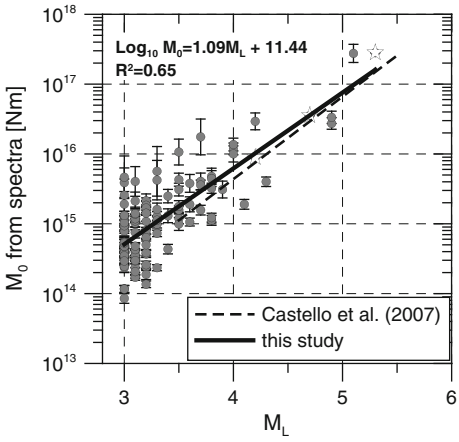

Fig. 7 Local magnitude (M_L) from the INGV-CNT bulletin versus seismic moment (M_0) estimated form the inverted source spectra. *Vertical bars* indicate the 95% confidence interval. The *black continuous line* represents the best least-squares fit. *Stars* are M_0 constrained to the values from RCMT

for these events. Consequently the regression has to be considered not well constrained in this study for such small magnitudes.

Finally, the seismic moment and corner frequency are used to determine the stress drop $\Delta\sigma$ and the source radius r using standard relationships (Keilis-Borok 1959; Brune 1970):

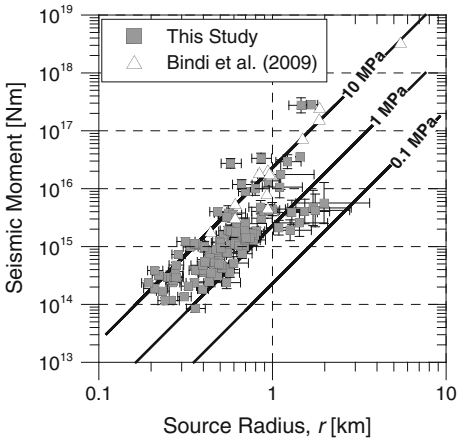

Fig. 8 Seismic moment versus source radius. *Vertical* and *horizontal bars* indicate the 95% confidence interval in the estimation of the relative parameters. The *black lines* represent constant stress drop relationships. Note that Bindi et al. (2009) used a radiation pattern of 0.63 and the source spectra are calculated for $\sqrt{NS^2 + EW^2 + Z^2}$ component of ground motion

$$r = \frac{2.34\beta}{2\pi f_c} \tag{6}$$

$$\Delta\sigma = \frac{7M_0}{16r^3} \tag{7}$$

Figure 8 shows the distribution of seismic moment versus source radius and compares it with constant stress drop scaling. The stress drops derived using Eq. (7) range from 0.3 to 60 MPa, with most of the values between 1 and 10 MPa. These results are in agreement with the typical worldwide values for normal and strike-slip faulting earthquakes over different seismic moments and tectonic environments (Kanamori 1994; Ruff 2002; Brune and Thatchaer 2002). We compared our estimates with values obtained by Bindi et al. (2009) for 13 events using strong-motion data, finding an overall good agreement between the two studies. The source spectra approximately follow self-similar scaling although it is clear that the bulk of data in this study comes from a restricted magnitude range ($3 \leq M \leq 4$) and this limits any general conclusions on this topic. Moreover some events with r larger than 1 are characterized by considerable uncertainties in r and M_0 estimation (see for instance the data points with stress drop between 0.1 and 1 Mpa in Fig. 8)

4.3 Site amplifications

As previously mentioned, in order to constrain the site response in the inversion, we considered the two stations located on rock site condition (i.e., GFZ05 and MI01) and computed the HVSR from the available records (55 for GFZ05 and 97 for MI01). The HVSR, presented in Fig. 9, show an approximately flat and low-amplitude amplification curve for GFZ05 while a clear peak at about 5 Hz is visible for MI01 station (see also Bergamaschi et al. this issue, for a detailed discussion on the topic). For this reason, in the inversion, we constrained the site response at GFZ05 to be equal to unity for both horizontal and vertical components.

In the following (Figs. 10, 11, 12 and 13) we will discuss the GIT site amplifications obtained for horizontal $\left(\text{i.e. } \sqrt{NS^2 + EW^2}\right)$ and vertical components and compare them with HVSR from earthquake recordings and seismic noise (only for velocimetric sensors).

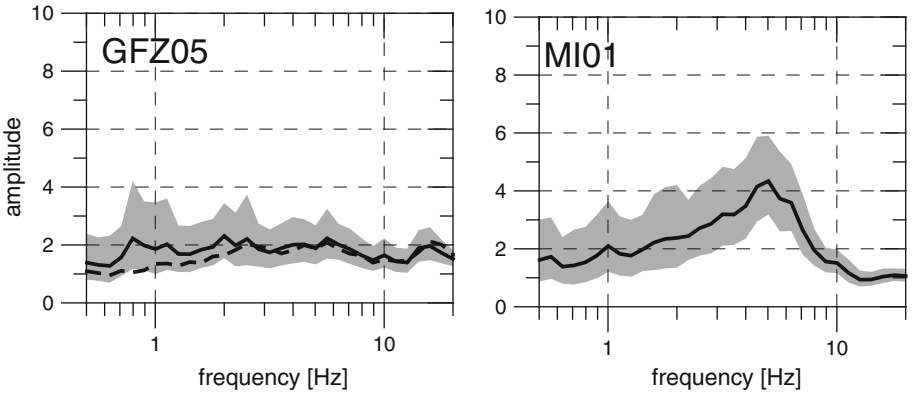

Fig. 9 HVSR at the rock stations GFZ05 (velocimetric) and MI01 (accelerometric) using 55 and 97 records, respectively. The *black continuous lines* and *gray shaded areas* mark the mean and standard deviation of the distribution. The *dashed black line* is the mean HVSR computed from pre-event noise windows

We prefer to present the GIT amplification curves separately for horizontal and vertical components (rather than computing the H-to-V GIT ratio) in order to highlight possible amplifications of the vertical component that will cause problems in the interpretation of the HVSR curves. Moreover, for reader convenience, we grouped the station according to their network.

The HVSR (mean $\pm$ standard deviation) are computed for each station with the same number of earthquake records used in the GIT inversion (see Table 1). For velocimetric stations, the HVSR from pre-event noise windows of the same length of S-wave windows are also calculated.

The results show that for some stations there is a quite good agreement between the HVSR and the GIT horizontal (GIT H) amplification curves, however, there are also remarkable differences that we will discuss later. These results are consistent with HVSR and standard spectral ratios (SSR) presented by Bergamaschi et al. (this issue) considering the same stations (apart from the accelerometers) and reference site. It is worth mentioning that Bergamaschi et al. used a different dataset consisting of a substantially smaller number of events (18 events) located about 20 km NW to the city of L'Aquila (in the Campotosto area). Moreover they selected S-waves windows of fixed length of 10 s, whereas we based our selection on the 90% percent energy band and allow a maximum duration of 15 s (see Dataset section). The agreement between their and our HVSR curves suggests that the different processing and source-to-site azimuths and distances sampled in the adopted datasets do not significantly affect, in this case, the HVSR calculation.

Examining Figs. 10, 11, 12 and 13 more in detail, it is striking that the GIT vertical (GIT V) curves are, in many cases, affected by amplification. As a consequence, the main differences between HVSR and GIT H appear at those stations where amplification of the vertical component is remarkable and, therefore, the assumption on which HVSR validity is based (i.e., absence of amplification of the vertical motion) fails. Other studies that apply the same inversion technique to different datasets also noticed amplifications of the vertical components (e.g., Castro et al. 1997; Parolai et al. 2004; Bindi et al. 2009; Oth et al. 2009, 2010).

The amplification results at some stations will be discussed with the aim to emphasize the misleading interpretation of HVSR due to amplification of the vertical component.

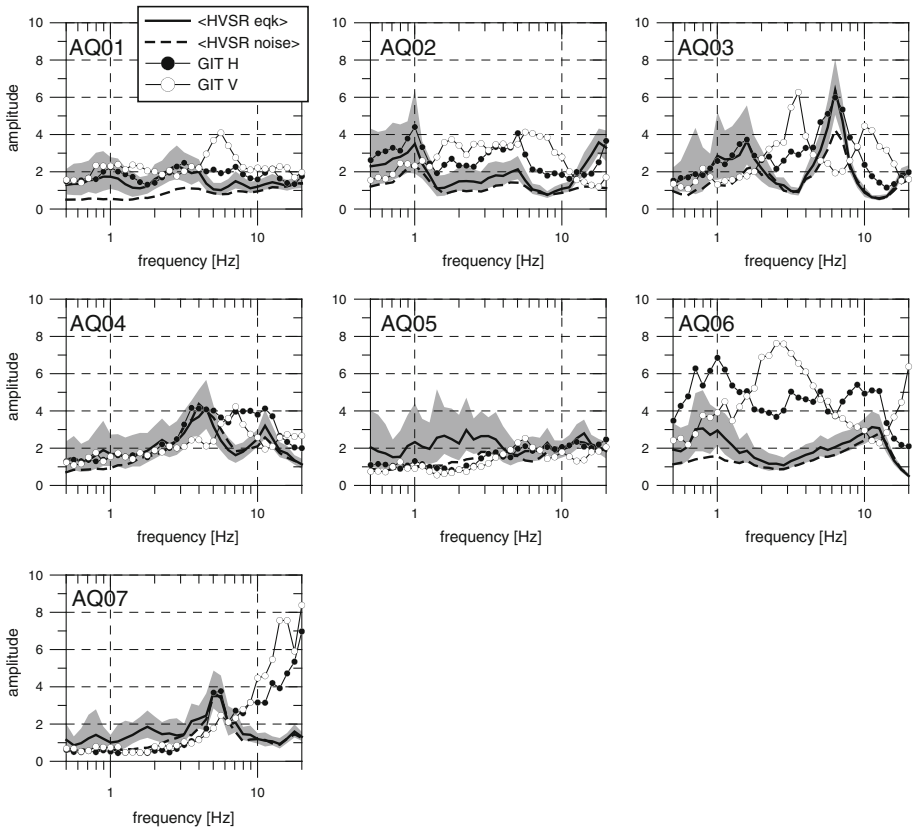

Fig. 10 Site amplification functions for the AQ (INGV-Rome) velocimetric stations. Mean site amplifications obtained from the GIT for horizontal (*black dots*) and vertical (*white dots*) components and considering HVSR from earthquakes recordings (*black thick lines*) and from noise windows on the pre-event portion of the signal (*dashed lines*). The *gray shaded* areas mark the mean ± one standard deviation of the HVSR from earthquakes recordings. The standard deviation of the 100 bootstrap sample for GIT amplifications is of the order of 0.04

AQ04 and AQ06 stations (Fig. 10) show HVSR curves characterized by two amplification peaks at about 4 and 10 Hz (AQ04) and 0.8 and 10 Hz (AQ06), separated by a trough. The GIT site amplifications reveal that at both sites the trough is fictitious due to amplification of the vertical component and that the horizontal amplifications are rather broadband between 4 to 10 Hz at AQ04 and 0.6 to 10 Hz at AQ06.

Stations MI03 and MI05 are two further interesting examples (Fig. 11). The HVSR peak at about 2 Hz at MI03 is in good agreement with the GIT H results, but, at higher frequencies, while the HVSR tends to flatten, the GIT H shows an increasing amplification with peaks at 5 and 10 Hz, where a maximum amplitude of 8 is obtained. This amplification at high frequencies is not observed in the HVSR due to amplification of the vertical component. The HVSR at MI05 shows two clear amplification peaks at about 2.5 and 8 Hz, the first one being of larger amplitude. On the other hand, the GIT H amplification curve provides larger amplitude for the second peak. Again, the reason for differences between the HVSR and GIT H curves appears to be the amplification of the vertical component, in this case, in correspondence on the second peak.

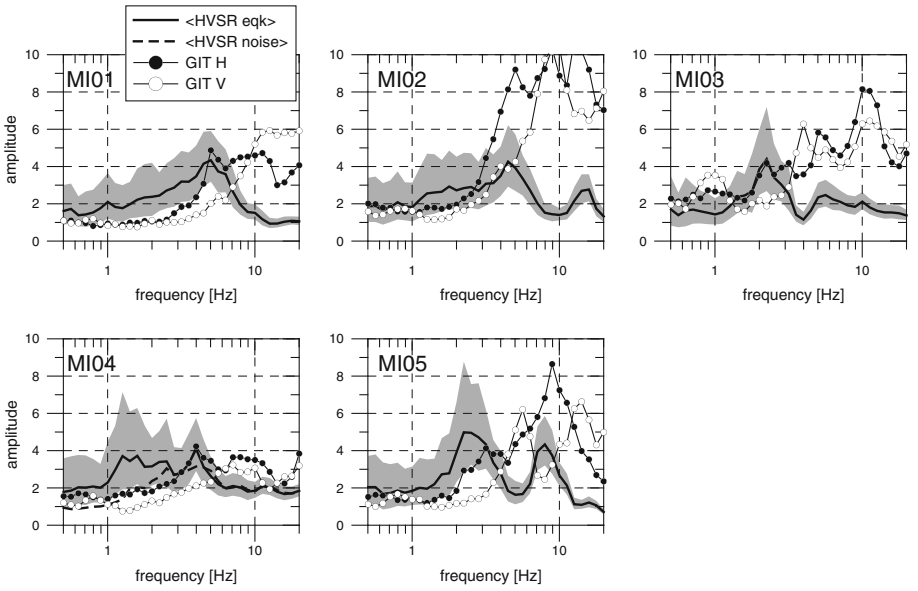

Fig. 11 Same as Fig. 10 but for the MI (INGV-Milan) accelerometric and velocimetric (only MI04) stations. Note that HVSR from noise is not calculated from accelerometric records. The standard deviation of the 100 bootstrap sample for GIT amplifications is of the order of 0.03

It is interesting to note that at MI02, a strong amplification at frequencies larger than 4 Hz is obtained for both GIT H and GIT V curves with amplitudes substantially larger than that obtained from HVSR.

Figure 12 shows the amplification curves for the AGFZ accelerometric stations. Note that these stations are mostly located south-east of the Aterno valley, except AGFZ07 and AGFZ10 located in the middle Aterno valley and north-west of L'Aquila city, respectively. It also important to mention that these stations, apart from AGFZ01 and AGFZ02, recorded a relatively small number of events (see Fig. 2; Table 1) compared to the other networks. Nevertheless, even though we are aware of the lower reliability of the site response results at these sites, we decided to include them in the dataset since they have not been considered by Bergamaschi et al. (this issue) and can be of interest for the study of the site response in the area. The HVSR curves show remarkable amplification levels and clear peaks between 1 and 3 Hz at 5 stations (AGFZ02, 03, 04, 05 and 07). However, while such amplifications are consistent with the GIT H results for AGFZ04 and AGFZ05 stations, for the remaining sites, the GIT H amplitudes are lower (i.e., at AGFZ07) or their maxima are at different frequencies (i.e., AGFZ02). AGFZ04 and AGFZ05 sites, where both HVSR and GIT H results agree on maximum amplifications of the order of 8–10 at 1 Hz, are located within the Castelnuovo village, about 20 km south-east of the L'Aquila mainshock epicenter, where the maximum macroseismic intensity (IX-X MCS degrees) has been reported after the 6 April 2009 event (Galli and Camassi 2009). At these sites, amplification of the vertical component is also observed, at frequencies larger than 2 Hz, leading to flat HVSR curves.

Finally, Fig. 13 shows the site response results for the three GFZ velocimetric stations. At GFZ01, HVSR and GIT H results are not in agreement and the trough observed in the HVSR seems to be, again, a consequence of the amplification of the vertical component. The GIT H curve shows, at this station, amplification for frequencies higher than 6 Hz. On

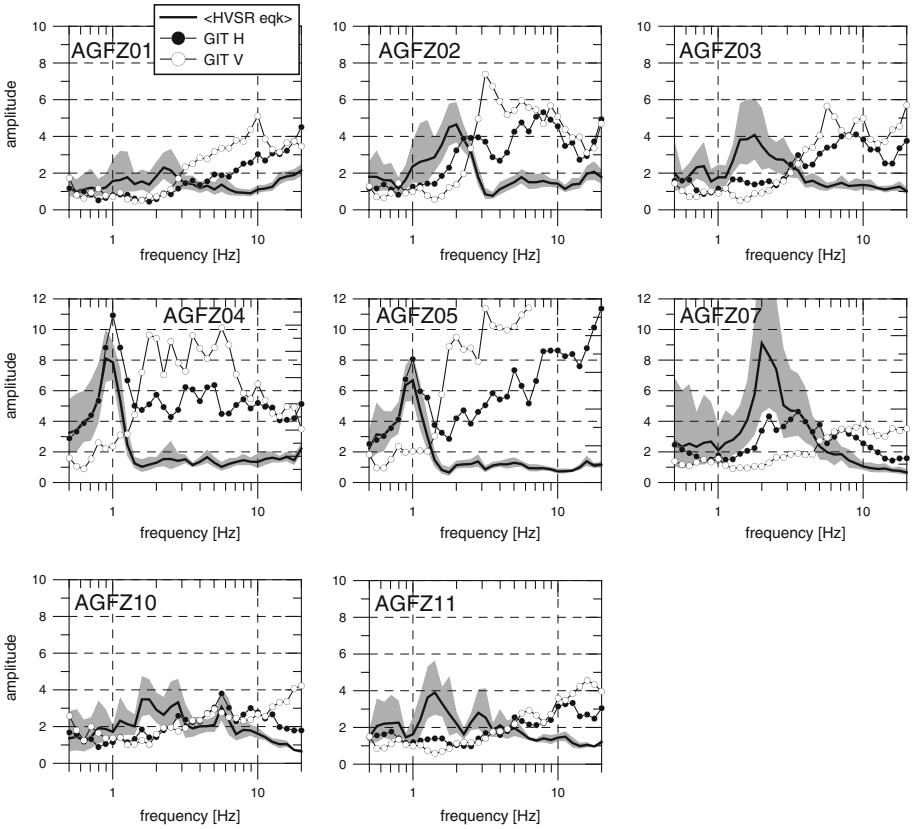

Fig. 12 Same as Fig. 10 but for the AGFZ (GFZ-Potsdam) accelerometric stations. Note that no HVSR from noise are calculated from accelerometric records. The standard deviation of the 100 bootstrap sample for GIT amplifications is of the order of 0.06

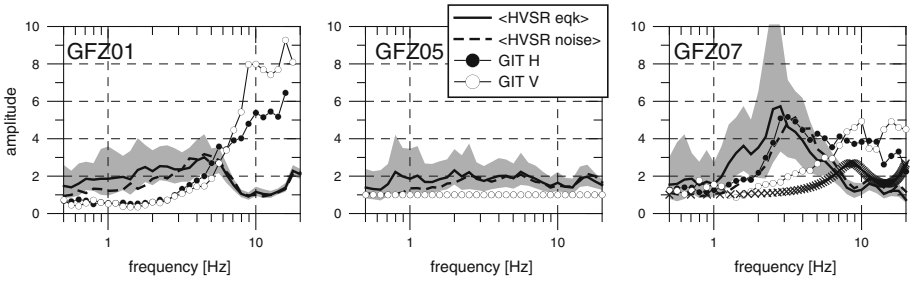

Fig. 13 Same as Fig. 10 but for the GFZ (GFZ-Potsdam) velocimetric stations. For GFZ07 station the frequency response of the SG5 soil profile to vertical incidence of P-waves (*black crosses*) is also shown (see text). The standard deviation of the 100 bootstrap sample for GIT amplifications is of the order of 0.03

the other hand, at GFZ07, the HVSR and GIT H results are in quite good agreement and the amplification peak is detected by both methods. Note that this station is located only few hundred meters from AGFZ07, where indeed, the same amplification features are observed.

The amplification of the vertical component of motion can be attributed to several factors: (i) S-P conversion at the bottom of the soft layer in the case of high-impedance contrasts (Parolai and Richwalski 2004); (ii) 2D or 3D effects at the edge of sedimentary basins or due to topography; (iii) presence of P-wave trains in the selected S-wave windows as the source-to-site distance is, in some cases, very short and the separation between P and S waves was not feasible. Moreover, the sources-to-sites geometry of this study implies a number of near-vertical ray paths due to the location of most of stations just above the hypocenters providing large P-waves amplitude.

For instance, the vertical amplifications at sites located in the Castelnuovo village (AGFZ04 and AGFZ05) can be caused by 2D effects due to the morphological characteristics of the relief where the village is established. Indeed, Castelnuovo is located on a hilltop 10–70 m above the surrounding alluvial plain. The hill has an elliptical shape and consists of conglomerates and sands of lower to medium Pleistocene age that lie on top of soft carbonate silt (Bosi and Bertini 1970; GEER 2009).

Vertical amplifications can also be obtained in case of 1D soil profiles considering P-wave incidence. In order to test this hypothesis in the study area, we took advantage of the 1D velocity profile derived from a down-hole test at S. Gregorio village (SG5, see Bergamaschi et al. this issue). The profile is close to station GFZ07 (Fig. 13) where amplification of the vertical component is obtained from GIT. Although the vertical amplifications are not large at this station, two peaks are visible at 10 and 15 Hz. Figure 13 (right plot) shows the frequency response of the SG5 soil profile to vertical incidence of P-waves (black crosses). The P-wave amplification function shows a good agreement with the GIT V curve: the frequency peak at about 10 Hz is visible for both curves, though somehow smaller amplitudes are obtained from the 1D profile.

5 Conclusions

In this article we presented the results obtained applying the Generalized Inversion Technique (GIT) to the data recorded by 23 temporary stations deployed in the Aterno valley during the 2009 L'Aquila seismic sequence. The GIT scheme allowed to separate source, path and site contributions in the recorded ground motions and to estimate source (i.e., seismic moment and stress drop) and attenuation (i.e., geometrical spreading and quality factor) parameters that are relevant for seismic hazard studies in the area. The proposed application of the GIT differs from that in most of the previous studies because we used events and stations located within a small area (about 30 km) from the L'Aquila mainshock epicenter. For this reason the collected dataset is characterized by a large number of records related to short hypocentral distances and the source-to-site paths densely sample the crustal volume below the Aterno valley. This allowed us to soundly estimate the attenuation properties of the shallow crust below L'Aquila.

The main results of this study are:

– the attenuation of S-waves from earthquakes located just below the Aterno valley (related to records with hypocentral distances roughly smaller than 13 km) is very pronounced. This can be related to waves traveling trough the highly heterogeneous and fractured crust in the fault zone of the L'Aquila earthquake. Considering distances within 30 km, when a

standard 1/R is used to account for the geometrical attenuation, the anelastic attenuation is found to be $Q_S = 23 f^{0.58}$. On the other hand when considering a distance-dependent geometrical spreading with a $1/R^3$ decay in the first 13 km (possibly related to the decay of the near-field terms), the Q_S is found to be more scattered, roughly equal to 100–200 and with a weak dependence on frequency.

- the nonparametric source spectra are satisfactorily explained using the omega-square model. The stress drop values derived for the considered events vary between 0.3 and 60 MPa with a mean value of 3.3 ± 2.8 MPa. These results are in agreement with the worldwide range of normal and strike-slip faulting earthquakes over different seismic moments and tectonic environments (Kanamori 1994; Ruff 2002; Brune and Thatchaer 2002). The source parameters estimated by Bindi et al. (2009) for the 13 events with $M_w > 4$ of the sequence are also in agreement with our results, though they found a slightly larger average stress drop of 9.4 Mpa. The stress drop values estimated from this study are also consistent with values obtained from aftershocks of the 1997–1998 Umbria-Marche seismic sequence in the magnitude range 1.4–4.5 for which an average stress drop of 3.8 ± 1.0 has been reported (Bindi et al. 2001).
- we used the M_L provided by the INGV-CNT Bulletin for 102 earthquakes considered in this study and the seismic moment determined with the GIT to derive a $M_0 - M_L$ relation. The equation is in good agreement with that derived for the Italian territory using data collected between 1997 and 2002 (Castello et al. 2007).
- the amplification levels determined by the GIT confirm the large variability of site response over the study area with significant peaks in the frequency range from 1 to more than 10 Hz. We found that the vertical component of the motion is amplified at a number of sites where, as a consequence, the HVSR method can fail in detecting the amplitude levels and in some cases the resonance frequencies. The amplification of the vertical motion can be ascribed to different causes and further and detailed analyses should be carried out to discern among them. Based on independent information available for some sites, we argue that vertical amplifications at AGFZ04 and AGFZ05 sites located in the village of Castelnuovo are due to topographic effects. Moreover, we used the 1D velocity profile derived from down-hole measurements close to station GFZ07 (S.Gregorio village) to verify that the vertical amplification obtained by GIT at the station can be due to S-P conversions in the soil profile or to the presence of P-waves in the selected signal windows.

Acknowledgments This work has been supported by the DPC-INGV S4 (2007–2009) project. We thank Raul R. Castro and Danilo Galluzzo for the valuable comments and suggestions that improve the quality of the paper. Roberto Paolucci kindly provided the "PSVQ" program to calculate the plane-wave response of a layered model. The Authors are grateful to the following individuals which were involved in the collection and interpretation of experimental data: Francesco Bergamaschi, Riccardo Mario Azzara, Paolo Augliera, Paola Bordoni, Fabrizio Cara, Rocco Cogliano, Ezio D'Alema, Domenico Di Giacomo, Giuseppe Di Giulio, Antonio Fodarella, Gianlorenzo Franceschina, Fabrizio Galadini, Maria Rosaria Gallipoli, Stefano Gori, Paolo Harabaglia, Chiara Ladina, Sara Lovati, Simone Marzorati, Marco Massa, Giuliano Milana, Francesca Pacor, Matteo Picozzi, Stefania Pucillo, Rodolfo Puglia, Gaetano Riccio, Monika Sobiesiak and Angelo Strollo.

Appendix

See Table 2.

Table 2 Source parameters of the considered earthquakes. M_w and $\Delta\sigma$ are estimated in this study

Event ID	Date	UTC time	ML	Lat (°)	Lon (°)	Depth (km)	MW	Δs (Mpa)
1	07/04/2009	9.26.28	4.7	42.34	13.39	10.2	5.0	5.17
2	07/04/2009	9.30.56	3.5	42.33	13.36	10	4.3	2.11
3	07/04/2009	10.29.10	3.2	42.32	13.4	9.5	3.9	2.67
4	07/04/2009	12.29.00	3.3	42.46	13.41	8.3	4.0	1.25
5	07/04/2009	17.47.37	5.3	42.28	13.46	15.1	5.6	25.81
6	07/04/2009	21.34.29	4.2	42.38	13.38	7.4	4.6	11.50
7	07/04/2009	21.39.06	3.7	42.36	13.36	10.4	4.4	2.50
8	07/04/2009	22.29.50	3.1	42.28	13.49	9.6	4.0	1.35
9	07/04/2009	22.43.42	3	42.33	13.49	9.3	4.2	0.38
10	08/04/2009	3.00.34	3.5	42.3	13.46	10	4.7	3.49
11	08/04/2009	4.27.41	3.7	42.31	13.47	10.7	4.8	5.53
12	08/04/2009	10.34.09	3.1	42.35	13.38	9.2	4.0	2.50
13	08/04/2009	11.35.57	3.5	42.36	13.33	10.6	4.0	1.73
14	08/04/2009	13.02.28	3.1	42.5	13.36	9.6	3.6	0.65
15	08/04/2009	17.58.35	3.2	42.36	13.4	8.8	4.1	1.52
16	08/04/2009	21.11.04	3.1	42.3	13.57	10.1	4.4	0.49
17	08/04/2009	22.56.50	4.3	42.51	13.36	10.2	4.4	15.38
18	08/04/2009	23.18.06	3.3	42.39	13.33	10.8	4.1	2.33
19	09/04/2009	0.52.59	5.1	42.48	13.34	15.4	5.6	38.74
20	09/04/2009	1.25.51	3.1	42.51	13.35	2.4	3.5	1.28
21	09/04/2009	2.37.26	3.1	42.5	13.34	10.4	3.7	3.61
22	09/04/2009	3.14.52	4.2	42.34	13.44	18	4.9	7.07
23	09/04/2009	3.41.55	3.1	42.51	13.33	9.8	3.6	8.29
24	09/04/2009	4.29.45	3.2	42.5	13.35	11	3.6	5.52
25	09/04/2009	4.32.44	4	42.45	13.42	8.1	4.7	17.61
26	09/04/2009	4.43.09	3.7	42.51	13.37	9.2	4.1	4.68
27	09/04/2009	6.10.29	3.1	42.49	13.4	9.4	3.5	5.92
28	09/04/2009	9.31.06	3	42.36	13.39	8.8	3.8	2.92
29	09/04/2009	13.00.29	3	42.3	13.47	9.9	4.4	0.79
30	09/04/2009	13.19.33	3.6	42.34	13.26	10	4.4	9.60
31	09/04/2009	15.18.14	3.2	42.31	13.5	10	4.1	4.67
32	09/04/2009	19.38.16	4.9	42.5	13.36	17.2	4.9	63.29
33	09/04/2009	20.47.01	3.1	42.49	13.31	10	3.6	12.87
34	09/04/2009	21.09.49	3	42.51	13.34	9.6	3.5	2.30
35	09/04/2009	22.40.06	3.6	42.48	13.3	10.9	4.0	9.06
36	10/04/2009	3.22.22	3.7	42.47	13.42	9.4	4.3	7.62
37	10/04/2009	4.33.04	3.3	42.46	13.35	10.5	3.9	13.50
38	10/04/2009	6.41.31	3	42.52	13.34	9.3	3.6	1.34
39	10/04/2009	11.53.09	3.1	42.24	13.48	9.6	4.0	4.29
40	10/04/2009	15.22.43	3	42.25	13.48	10.2	3.9	4.34
41	10/04/2009	15.46.17	3.3	42.35	13.38	9.9	4.0	11.34
42	10/04/2009	19.07.21	3.1	42.38	13.39	9.5	4.0	2.22

Table 2 continued

Event ID	Date	UTC time	ML	Lat (°)	Lon (°)	Depth (km)	MW	Δs (Mpa)
43	10/04/2009	19.18.39	3	42.34	13.36	10.2	3.7	1.23
44	11/04/2009	5.39.00	3.3	42.39	13.4	10.7	4.0	10.36
45	11/04/2009	6.13.26	3	42.47	13.42	9.1	3.7	2.42
46	11/04/2009	6.57.02	3.2	42.39	13.41	10.5	3.9	3.15
47	11/04/2009	7.04.14	3.2	42.39	13.41	11	4.0	2.55
48	11/04/2009	15.42.29	3.1	42.52	13.32	8.7	3.7	0.83
49	11/04/2009	19.53.53	3	42.35	13.53	9.8	4.4	0.40
50	12/04/2009	3.29.35	3.1	42.54	13.32	9.7	3.5	2.55
51	12/04/2009	9.48.58	3.2	42.36	13.38	10.1	4.2	3.91
52	12/04/2009	16.35.53	3.2	42.52	13.38	10.1	3.6	5.93
53	12/04/2009	18.05.16	3.4	42.4	13.39	9.8	4.0	1.22
54	12/04/2009	18.09.42	3	42.29	13.5	10.4	3.7	2.64
55	13/04/2009	1.01.44	3	42.24	13.5	9.2	3.9	3.63
56	13/04/2009	7.08.30	3.1	42.27	13.48	9.3	3.9	1.10
57	13/04/2009	8.41.08	3	42.27	13.51	9.9	3.9	2.10
58	13/04/2009	13.36.04	3.4	42.44	13.44	9	4.2	3.22
59	13/04/2009	18.11.25	3	42.55	13.3	10.7	3.3	2.87
60	13/04/2009	19.09.49	3.8	42.36	13.35	10.4	4.4	3.34
61	13/04/2009	19.17.57	3.5	42.36	13.35	11.3	4.1	1.40
62	13/04/2009	20.08.24	3	42.37	13.37	10.5	3.8	1.05
63	13/04/2009	21.14.24	4.9	42.5	13.36	7.5	5.0	23.08
64	14/04/2009	7.36.44	3	42.5	13.4	10.1	3.6	1.20
65	14/04/2009	9.08.07	3.2	42.26	13.49	10.6	3.8	3.37
66	14/04/2009	13.56.21	3.9	42.54	13.31	10	4.3	6.94
67	14/04/2009	17.27.30	3.5	42.53	13.3	3.6	4.0	6.54
68	14/04/2009	19.28.02	3.4	42.54	13.31	11	3.7	1.96
69	14/04/2009	20.17.27	4.1	42.53	13.29	10.4	4.2	4.83
70	14/04/2009	20.53.09	3.1	42.55	13.3	9.2	3.6	7.37
71	15/04/2009	11.44.40	3	42.29	13.47	10.7	4.0	4.02
72	15/04/2009	15.23.46	3	42.46	13.37	9.9	3.3	0.80
73	15/04/2009	19.36.44	3.2	42.52	13.29	6.3	3.5	8.92
74	15/04/2009	19.55.57	3	42.47	13.37	9.3	3.6	6.51
75	15/04/2009	22.53.07	3.8	42.51	13.31	8.6	4.0	10.99
76	16/04/2009	5.44.54	3.2	42.29	13.4	9.9	4.1	4.29
77	16/04/2009	16.11.37	3	42.55	13.3	11.1	3.3	3.64
78	16/04/2009	17.49.30	3.8	42.54	13.29	10.9	4.0	17.09
79	18/04/2009	9.05.56	3.8	42.44	13.36	14.6	4.3	8.69
80	18/04/2009	11.07.21	3.2	42.27	13.49	9.4	4.1	1.66
81	18/04/2009	13.03.08	3.1	42.33	13.5	10.2	4.2	0.72
82	20/04/2009	2.22.15	3	42.38	13.32	10.5	3.7	1.75
83	20/04/2009	7.13.14	3.1	42.41	13.35	10.1	3.7	1.38
84	20/04/2009	11.43.06	3	42.28	13.5	9.9	3.8	1.58
85	21/04/2009	15.44.36	3.6	42.33	13.37	10.7	4.2	2.51

Table 2 continued

Event ID	Date	UTC time	ML	Lat (°)	Lon (°)	Depth (km)	MW	Δs (Mpa)
86	21/04/2009	16.20.56	3.2	42.51	13.31	12	3.4	1.99
87	23/04/2009	15.14.08	4	42.25	13.49	9.9	4.6	8.74
88	23/04/2009	21.49.00	4	42.23	13.48	9.3	4.7	7.01
89	24/04/2009	4.36.17	3	42.26	13.47	10.3	3.9	3.20
90	24/04/2009	13.38.53	3.2	42.52	13.35	9.4	3.7	7.71
91	24/04/2009	14.24.07	3	42.39	13.39	8.3	4.2	0.42
92	24/04/2009	15.53.45	3	42.31	13.47	10.5	4.0	2.13
93	24/04/2009	22.51.29	3	42.27	13.51	11	4.0	1.75
94	25/04/2009	2.08.23	3.1	42.29	13.45	8.3	4.1	1.73
95	25/04/2009	11.13.04	3	42.42	13.33	9.1	3.6	5.95
96	25/04/2009	13.17.31	3	42.26	13.5	10.9	3.8	3.33
97	26/04/2009	17.56.06	3.3	42.46	13.38	10.6	3.5	14.21
98	29/04/2009	8.57.42	3	42.25	13.49	9.4	3.8	3.52
99	30/04/2009	9.13.55	3	42.37	13.42	9.6	3.8	2.34
100	30/04/2009	13.01.01	3.5	42.36	13.36	10.9	4.1	3.33
101	01/05/2009	5.12.51	3.8	42.28	13.47	9	4.4	1.97
102	01/05/2009	20.34.44	3.3	42.33	13.5	10	4.4	0.34
103	02/05/2009	2.21.02	3.2	42.5	13.36	9.7	3.7	18.14
104	02/05/2009	20.15.00	3.3	42.3	13.5	9.4	4.5	0.32
105	03/05/2009	5.14.43	3.2	42.37	13.39	10.1	3.8	1.85
107	05/05/2009	10.44.03	3	42.28	13.5	10.3	4.0	1.73
108	05/05/2009	18.03.41	3.1	42.27	13.51	10.1	4.1	1.49
110	09/05/2009	9.09.40	3.2	42.35	13.36	10.5	4.1	1.78
111	10/05/2009	16.00.07	3.5	42.3	13.48	10	4.4	2.16
112	11/05/2009	16.59.04	3.1	42.49	13.37	9.8	3.8	9.72

The other parameters are from INGV-CNT Bulletin (http://cnt.rm.ingv.it)

References

Aki K, Richards PG (1980) Quantitative seismology: theory and methods, vols 1 and 2. W. H. Freeman, San Francisco 932

Andrews DJ (1986) Objective determination of source parameters and similarity of earthquakes of different size. In: Das S, Boatwright J, Scholz CH (eds) Earthquake source mechanics. American Geophysical Union, Washington

Bergamaschi F, Cultrera G, Luzi L, Azzara RM, Ameri G, Augliera P, Bordoni P, Cara F, Cogliano R, D'Alema E, Di Giacomo D, Di Giulio G, Fodarella A, Franceschina G, Galadini F, Gallipoli MR, Gori S, Harabaglia P, Ladina C, Lovati S, Marzorati S, Massa M, Milana G, Mucciarelli M, Pacor F, Parolai S, Picozzi M, Pilz M, Puglia R, Pucillo S, Riccio G, Sobiesiak M (2010) Evaluation of site effects in the Aterno river valley (Central Italy) from the aftershocks of the 2009 L'Aquila earthquake recorded by a temporary seismic network. Bull Earth Eng (this issue)

Bindi D, Spallarossa D, Augliera P, Cattaneo M (2001) Source parameters estimated from the aftershocks of the 1997 Umbria–Marche (Italy) seismic sequence. Bull Seismol Soc Am 91:448–455

Bindi D, Castro RR, Franceschina G, Luzi L, Pacor F (2004) The 1997–1998 Umbria–Marche sequence (Central Italy): source, path and site effects estimated from strong motion data recorded in the epicentral area. J Geophys Res 109:B04312. doi:10.1029/2003JB002857

Bindi D, Pacor F, Luzi L, Massa M, Ameri G (2009) The M_w6.3, 2009 L'Aquila earthquake: source, path and site effects from spectral analysis of strong motion data. Geophys J Int 179:1573–1579. doi:10.1111/j.1365-246X.2009.04392.x

Bonilla LF, Steidl JH, Lindley GT, Tumarkin AG, Archuleta RJ (1997) Site amplification in the San Fernando Valley, California: variability of site-effect estimation using the S-wave, coda and H/V methods. Bull Seismol Soc Am 87:710–730

Bosi C, Bertini T (1970) Geologia della media valle dell'Aterno. Mem Soc Geol It IX:719–777

Brune JN (1970) Tectonic stress and the spectra of seismic shear waves from earthquakes. J Geophys Res 75:4997–5009

Brune JN, Thatchaer W (2002) Strength and energetics of active fault zones. In: Lee WHK et al (ed) Earthq Eng Seismol. Academic, San Diego pp 569–588

Cantore L, Oth A, Parolai S, Bindi D (2011) Attenuation, source parameters and site effects in the Irpinia-Basilicata region (southern Apennines, Italy). J Seismol (in press)

Castro RR, Anderson JG, Singh SK (1990) Site response, attenuation and source spectra of S waves along the Guerrero, Mexico, subduction zone. Bull Seismol Soc Am 80:1481–1503

Castro RR, Mucciarelli M, Pacor F, Petrungaro C (1997) S-Wave site-response estimates using horizontal-to-vertical spectral ratios. Bull Seismol Soc Am 87:256–260

Castro RR, Massa M, Augliera P, Pacor F (2008) Body-wave Attenuation in the Region of Garda, Italy. Pure Appl Geophys 165:1351–1366

Castello B, Olivieri M, Selvaggi G (2007) Local and duration magnitude determination for the Italian Earthquake Catalog, 1981–2002. Bull Seismol Soc Am 97:128–139

Chiarabba C, Amato A, Anselmi M, Baccheschi P, Bianchi I, Cattaneo M, Cecere G, Chiaraluce L, Ciaccio MG, De Gori P, De Luca G, Di Bona M, Di Stefano R, Faenza L, Govoni A, Improta L, Lucente FP, Marchetti A, Margheriti L, Mele F, Michelini A, Monachesi G, Moretti M, Pastori M, Piana Agostinetti N, Piccinini D, Roselli P, Seccia D, Valoroso L (2009) The 2009 L'Aquila (central Italy) M_w6.3 earthquake: main shock and aftershocks. Geophys Res Lett 36:L18308. doi:10.1029/2009GL039627

Cultrera G, Luzi L, Ameri G, Augliera P, Azzara RM, Bergamaschi F, Bertrand E, Bordoni P, Cara F, Cogliano R, D'Alema E, Di Giacomo D, Di Giulio G, Duval AM, Fodarella A, Franceschina G, Gallipoli MR, Harabaglia P, Ladina C, Lovati S, Marzorati S, Massa M, Milana G, Mucciarelli M, Pacor F, Parolai S, Picozzi M, Pilz M, Puglia R, Pucillo S, Régnier J, Riccio G, Salichon J, Sobiesiak M (2009) Evaluation of the local site effects in the upper and middle Aterno valley Numero speciale Abruzzo. Seismic Action and site effects, Progettazione sismica, n.03 2009. IUSS Press, ISSN 1973-7432

Drouet S, Chevrot S, Cotton F, Souriau A (2008) Simultaneous inversion of source spectra, attenuation parameters, and site responses: application to the data of the French accelerometric network. Bull Seismol Soc Am 98:198–219

Field EH, Jacob KH (1995) A comparision and test of various site-response estimation techniques, including three that are not refernce-site dependent. Bull Seism Soc Am 4:1127–1143

Galli P, Camassi R (eds) (2009) Rapporto sugli effetti del terremoto aquilano del 6 Aprile 2009, Rapporto congiunto DPC-INGV, 12 pp. Available at: http://portale.ingv.it/real-time-monitoring/quest/aquilano-06-04-2009/

GEER (Sep, 2009) Preliminary report on the seismological and geotechnical aspects of the April 6 2009 L'Aquila earthquake in central Italy (Version 2.0). Association Report No. GEER-016. National Science Foundation-Sponsored GeoEngineering Extreme Events Reconnaissance (GEER) Team. http://www.geerassociation.org/

Hanks TC, Kanamori H (1979) A moment-magnitude scale. J Geophys Res 84:2348–2350

Kanamori H (1994) Mechanics of earthquakes. Ann Rev Earth Planet Sci 22:207–237

Keilis-Borok V (1959) On the estimation of the displacement in an earthquake source and of source dimension. Ann Geofis 12:205–214

Konno K, Ohmachi T (1998) Ground-motion characteristics estimated from spectral ratio between horizontal and vertical components of microtremor. Bull Seismol Soc Am 88:228–241

Lermo J, Chavez-Garcia FJ (1993) Site effect evaluation using spectral ratios with only one station. Bull Seismol Soc Am 83:1574–1594

Malagnini L, Akinci A, Mayeda K, Munafo' I, Herrmann RB, Mercuri A (2010) Characterization of earthquake-induced ground motion from the L'Aquila seismic sequence of 2009, Italy. Geophys J Int 184:325–337

Menke W (1989) Geophysical data analysis: discrete inverse theory. Academic Press, New York

Nakamura Y (1989) A method for dynamic characteristics estimation of subsurface using microtremor on the ground surface. QR Railw Tech Res Inst 30:25–33

Oth A, Bindi D, Parolai S, Wenzel F (2008) S-wave attenuation characteristics beneath the Vrancea region in Romania: new insights from the inversion of ground-motion spectra. Bull Seismol Soc Am 98:2482–2497

Oth A, Bindi D, Parolai S, Di Giacomo D (2010) Spectral analysis of K- and KiK-net data in Japan: II—on attenuation characteristics, source parameters and site response of borehole and surface stations. Bull Seismol Soc Am (in press)

Oth A, Parolai S, Bindi D, Wenzel F (2009) Source spectra and site response from S waves of intermediate-depth Vrancea, Romania, earthquakes. Bull Seismol Soc Am 99:235–254

Parolai S, Bindi D, Augliera P (2000) Application of the generalized inversion technique (GIT) to a microzonation study: numerical simulations and comparison with different site-estimation techniques. Bull Seismol Soc Am 90:286–297

Parolai S, Bindi D, Baumbach M, Grosser H, Milkereit C, Karakisa S, Zunbul S (2004) Comparison of different site response estimation techniques using aftershocks of the 1999 Izmit earthquake. Bull Seismol Soc Am 94:1096

Parolai S, Richwalski SM (2004) The importance of converted waves in comparing H/V and RSM site response estimates. Bull Seismol Soc Am 94:304–313

Piana Agostinetti N, Amato A (2009) Moho depth and Vp/Vs ratio in peninsular Italy from teleseismic receiver functions. J Geophys Res 114:B06303. doi:10.1029/2008JB005899

Ponziani F, De Franco R, Minelli G, Biella G, Federico C, Pialli G (1995) Crustal shortening and duplication of the Moho in the Northern Appennines: a view from seismic refraction data. Tectonophysics 252:391–418

Rovelli A, Bonamassa O, Cocco M, Di Bona M, Mazza S (1988) Scaling laws and spectral parameters of the ground motions in active extensional areas in Italy. Bull seism Soc Am 78:530–560

Ruff LJ (2002) State of stress within the earth. In: Lee WHK et al (ed) Earthquake and engineering seismology. Academic, San Diego pp 539–557

Salazar W, Sardina V, de Cortina J (2007) A hybrid inversion technique for the evaluation of source, path, and site effects employing S-wave spectra for subduction and upper-crustal earthquakes in El Salvador. Bull Seismol Soc Am 97:208–221

Seber GAF, Wild CJ (2003) Nonlinear regression. Wiley, Hoboken

Tucker B, King J (1984) Dependence of sediment-filled valley response on input amplitude and valley properties. Bull Seism Soc Am 74:153–165